Catalysis Today 144 (2009) 201–211

Contents lists available at ScienceDirect

Catalysis Today

journal homepage: www.elsevier.com/locate/cattod

Investigation of palladium interaction with cerium oxide and its state in catalysts for low-temperature CO oxidation

A.I. Boronin [a,b,*], E.M. Slavinskaya [a], I.G. Danilova [a], R.V. Gulyaev [a], Yu.I. Amosov [a], P.A. Kuznetsov [a], I.A. Polukhina [a], S.V. Koscheev [a], V.I. Zaikovskii [a], A.S. Noskov [a]

[a] Boreskov Institute of Catalysis SB RAS, Pr. Akad. Lavrentieva 5, Novosibirsk 630090, Russia
[b] Novosibirsk State University, Pirogova 2, Novosibirsk 630090, Russia

ARTICLE INFO

Article history:
Available online 24 February 2009

Keywords:
Palladium
Ceria
Catalysis
CO oxidation
XPS
HRTEM
IRS

ABSTRACT

Palladium catalysts supported on nanosized CeO_2 supports were synthesized by different methods. The catalysts showed high low-temperature activity (LTA) in CO oxidation. The synthesized palladium–ceria catalysts for low-temperature CO oxidation were investigated by a complex of physicochemical methods, and their catalytic performance was determined in the light-off regime. It was shown using high-resolution transmission electron microscopy (HRTEM) and EDX microanalysis that the catalysts with high LTA are characterized by exceptionally high dispersity of palladium on the surface of the supports. Two different states of palladium were observed by XPS. They correspond to the surface interaction phases (SIPs) as $Pd_xCeO_{2-\delta}$ and small metal clusters (<10 Å). According to diffraction images obtained by HRTEM, the latter have flattened shape due to epitaxial binding between (1 1 1) facets of palladium and CeO_2. Two types of CO adsorption sites (Pd^{2+} and Pd^0) were distinguished by FTIR. They can be attributed to SIP (Pd^{2+}) and palladium in flat metal clusters ($Pd^{\delta+}$ and Pd^0). The drop of LTA in CO oxidation is related to the loss of the palladium chemical interaction with the surface of the support and palladium sintering to form PdO nanoparticles. The formation of PdO particles is stimulated by crystallization of CeO_2 particle surface due to the calcination of support at temperatures above 600 °C. The XPS, HRTEM and FTIR data give reliable evidence that PdO particles are not responsible for LTA in CO oxidation.

In this work, the structure of the active sites consisting of two phases: atomically dispersed palladium within the SIP and palladium metal nanoclusters is proposed. The catalyst pretreatment in hydrogen was found to improve significantly its catalytic (LTA) properties. The effect of the hydrogen pretreatment was supposed to be related to the formation of hydroxyl groups and their effect on the electronic and geometrical state of the surface active sites and their possible direct participation in CO oxidation.

© 2009 Elsevier B.V. All rights reserved.

1. Introduction

Palladium–ceria supported catalysts attract significant attention of researchers in relation to the fundamental aspects of their action as neutralizers of exhaust gases [1,2]. Industrial catalysts, for example, three-way conversion catalysts (TWC), have complex composition. However, palladium and cerium oxides are their basic components and play almost indispensable role in deep oxidation of CO and hydrocarbons at low temperatures ($T < 150$ °C).

The low-temperature activity (LTA) of deep oxidation catalysts is not typical of either palladium or ceria separately. A synergetic effect is observed only when palladium is supported on ceria. Ceria has been claimed to be a strong promoter of structural and electronic properties of catalysts both in the automotive pollution control and for a number of industrial processes, such as purification and reforming of CH_4, steam reforming of CO, CO_2, methanol, and diethyl ether [3–5], as well as PROX reaction [6,7]. Wide application of ceria in deep oxidation reactions is related to its ability to easily donate and accept oxygen atoms [8].

Palladium is one of the most active metals interacting with the surface of oxides. It is also characterized by relatively high oxygen affinity. However, at temperatures below 200 °C its oxidation to PdO_x phases that could account for the low-temperature activity is not yet observed [9–11]. CO oxidation on palladium metal is known to follow the Langmuir–Hinshelwood mechanism. The light-off temperature within this mechanism is largely determined by the CO adsorption energy [12–14]. Usually, CO adsorption energy on platinum metals, including palladium, is relatively high, varying in

* Corresponding author at: Boreskov Institute of Catalysis SB RAS, Pr. Akad. Lavrentieva 5, Novosibirsk 630090, Russia. Tel.: +7 383 3269 537; fax: +7 383 3308 056.
E-mail address: boronin@catalysis.ru (A.I. Boronin).

0920-5861/$ – see front matter © 2009 Elsevier B.V. All rights reserved.
doi:10.1016/j.cattod.2009.01.035

the range of 25–35 kcal/mol depending on the particle morphology and size. So, CO oxidation begins at $T > 200$–250 °C [9,15]. Strongly oxidized palladium in the form of PdO particles does not show low-temperature catalytic activity [9,16]. The deposition of dispersed palladium on inert or weakly interacting supports such as SiO_2 or Al_2O_3 decreases the light-off temperature. However, T_{50} is usually not lower than 130–150 °C [17]. The low-temperature activity appears only after deposition of palladium on oxides with variable oxidation state due to the interaction of Pd with the support surface. Thus, the low-temperature oxidation of CO over Pd/CeO_2 catalyst can be characterized by RedOx or Mars–Van Krevelen mechanisms [18].

Despite impressive technological achievements in development of deep oxidation catalysts, many fundamental aspects of catalytic action, first of all, the low-temperature oxidation mechanism, are still not developed. In the literature there are no unambiguous data on the electronic and structural state of the active component that are needed for the optimal catalyst. The key question is the interaction of the active component with the promoter – cerium oxide. This includes determination of the surface compounds and phases and their redox ability. These aspects are discussed in a number of papers [19–21]. However, there are still incomplete experimental data obtained by spectral and structural methods together with kinetic data. The formation of mixed palladium–cerium compounds is proposed in many studies. However, some researchers believe that the highly active in CO oxidation state of palladium is related to nanoparticles of palladium oxide PdO or dioxide PdO_2 localized inside the support oxide matrix [22–24]. Also, there is a controversial information concerning palladium in the reduced state. At this moment it is not clear whether palladium is in metallic or ionized state ($Pd^{\delta+}$, Pd^{1+}) after action of the reaction media or after action of reducing agents like CO or H_2. In general, there is no reliable understanding what kind of Pd–Ce–O species are the active ones in LTA of CO oxidation.

To answer the above questions, the application of a set of kinetic and physical methods is required. Such methods can aid in establishing a relation between electronic and geometrical structure of active component and the catalytic properties of Pd/CeO_2 system. In this work, the following methods were used: (a) the kinetic methods: light-off measurements and temperature programmed reaction TPR-CO—to obtain a correlation between reaction rate and oxygen mobility depending on temperature; (b) the spectroscopic methods: X-ray photoelectron spectroscopy (XPS), UV–vis DR and FTIR spectroscopy—to establish the atom charge and active component species; (c) the structural methods: X-ray diffraction (XRD) and transmission electron microscopy (TEM)—to characterize the structure of support and obtain information about local structure of active component and its distribution over the support surface.

Thus, the main objective of the present work is a detailed investigation of the palladium interaction with the support surface and determination of its electronic and structural state in the catalysts characterized by high low-temperature activity in CO oxidation. For this purpose, the Pd/CeO_2 catalysts with different catalytic activities were specially prepared by different methods. The results of this study were used to suggest a new model of active sites. It has a two-phase structure and a variable oxidation state of palladium (Pd^{2+}–Pd^0) on the CeO_2 surface that is required for the low-temperature CO oxidation. No large particles of Pd or PdO, which could be responsible for LTA in CO oxidation, are observed.

2. Experimental

2.1. Catalysts

The $1\%Pd/CeO_2$ catalysts used in the study differed in the method of ceria synthesis, palladium deposition, and thermal treatment in oxidizing or reducing environment.

CeO_2-T was prepared by $Ce(NO_3)_3$ thermolysis and calcined in air at 450, 600 or 800 °C for 4 h at each temperature.

CeO_2-P was prepared from a $Ce(NO_3)_3$ solution by precipitation in the form of oxycarbonates (precipitation with NH_4HCO_3) and calcined in air at 450 °C for 4 h.

Palladium deposition (1%) was carried out by two methods. The first method involved impregnation with a palladium nitrate $Pd(NO_3)_2$ solution. The samples prepared by the first method were designated as $Pd(N)/CeO_2$-T and $Pd(N)/CeO_2$-P. The second method included impregnation with a $Pd(NO_3)_2$ solution in the presence of acetic acid. The samples prepared by this method were denoted as $Pd(N + A)/CeO_2$-T and $Pd(N + A)/CeO_2$-P. Prior to the thermal treatment in redox environments, all the samples were dried at 110 °C for 12 h.

Before the catalytic tests, the samples were treated by two methods: treatment in 10% H_2/He flow while heating from ambient temperature to 450 °C or calcination in air at 450 °C. The supports have an index 450, 600 or 800 °C if they were calcined at these temperatures in air, and 450 °C-H_2 if they were treated in hydrogen.

2.2. Methods

The *catalytic properties* of the synthesized catalysts were studied in CO oxidation by oxygen using the light-off method and temperature programmed reaction with CO (TPR-CO). The experiments were carried out in an automated installation with a flow reactor and mass-spectrometric analysis of the gas phase. The sample (0.5–0.25 mm size) was placed into a stainless steel reactor. Then, the reaction mixture was fed either at 25 °C or at 0 °C. After that the sample was heated to 450 °C with 10 °C/min heating rate.

Light-off method. The reaction mixture had the following composition (vol.%): CO – 0.2, O_2 – 1.0, Ne – 0.5, helium the balance. Its flow rate was 1 l/min. The reaction mixture containing 0.2% CO and 1% O_2 was fed at room temperature on the catalyst sample. After a steady-state composition of CO, O_2 and CO_2 was reached, the sample was heated to 450 °C at 10 °C/min heating rate. The concentrations of CO, O_2 and CO_2 were measured at 0.34 Hz frequency.

TPR-CO method. The reaction mixture had the following composition (vol.%): CO – 1.0, Ne – 0.5, helium the balance. Its flow rate was 0.1 l/min. The reaction mixture containing 1% CO was introduced to the catalyst sample cooled in the reactor to 0 °C. After steady-state concentrations of CO and CO_2 were established, the sample was heated from 0 to 500 °C at 10 °C/min heating rate. The concentrations of CO and CO_2 were measured during the reaction.

XRD studies of the samples were carried out using a HZG-4C diffractometer with Cu Kα monochromated radiation.

HRTEM images were obtained using a JEM-2010 electron microscope (JEOL, Japan) with lattice-fringe resolution of 0.14 nm at the accelerating voltage of 200 kV. The high-resolution images of periodic structures were analyzed by the Fourier method. Local energy-dispersive X-ray analysis (EDXA) was carried out using an EDX spectrometer (EDAX Co.) fitted with a Si (Li) detector with the resolution of 130 eV. The samples for the HRTEM study were prepared on a perforated carbon film mounted on a copper grid.

Specific surface areas were determined using heat desorption of argon at ±10% accuracy.

X-ray photoelectron spectroscopy (*XPS*) study was carried out using an ES300 electron spectrometer (Kratos Analytical) with MgKα irradiation, $h\nu = 1253.6$ eV. For registration of the photoelectron spectra the samples were ground and deposited on an indium substrate. The use of an X-ray source with increased power

for several hours resulted in a considerable reduction of cerium oxide in agreement with the previous data [25,26]. To prevent ceria reduction, the spectra were registered at a lower X-ray power in the 10 kV × 5 mA working mode of the X-ray gun. The spectrometer was calibrated by a standard method relative to two lines, $Au4f_{7/2}$ and $Cu2p_{3/2}$, with binding energies 84.0 and 932.7 eV, respectively [27]. The spectra were calibrated using the U‴ component of the Ce3d line (BE = 916.7 eV). To determine the quantitative chemical composition and electronic state of the catalyst elements, precision spectra of the core photoelectron lines were registered with the 0.1 eV energy step using constant analyzer pass energy HV = 25. The spectra were obtained using an electron neutralizer and long accumulation time to improve precision for further spectroscopic processing. The electron neutralizer was tuned to obtain the position of the U‴ component in the spectrum close to 916.7 eV. The spectra were processed with a special WinCalc software that was successfully used for many other systems [28–30]. The chemical composition of the catalysts was calculated from integral intensities of the lines or their components with the account of the atomic sensitivity factors reported in [31]. The Pd3d and Ce3d spectra in all figures are presented in a normalized mode, that is, the spectra are normalized to the spectral background of all samples.

The *IR spectra* were measured using a Shimadzu FTIR-8300 spectrometer in the range of 700–6000 cm^{-1} with 4 cm^{-1} resolution. Each spectrum was scanned 100 times. The presented spectra were normalized to wafer density (ρ in g/cm^2). Before registration of the FTIR spectra, powdered samples were pressed in self-supported wafers ($\rho \approx 0.02$ g/cm^2). Then a wafer was placed in a quartz IR cell with NaCl windows and pretreated in air (673 K) and then under vacuum (298 K, $p < 10^{-6}$ bar). The CO adsorption was performed at 0.2 mbar (CO/Pd = ca. 3–5/1) and 10 mbar (in the presence of gas phase CO) at room temperature (absorption of gaseous CO was subtracted from the spectra).

Diffuse reflectance UV–vis spectra (UV–vis DRS) of the catalysts 1%Pd(N + A)/CeO_2-T-450 °C, 1%Pd(N + A)/CeO_2-T-600 °C, 1%Pd(N + A)/CeO_2-T-450 °C and corresponding supports were recorded using a UV-2501 PC Shimadzu spectrometer with IRS-250A diffusion reflection attachment in the 11,000–54,000 cm^{-1} range. The measurements were performed in a 2-mm quartz cell in air at room temperature. The UV–vis spectra were transformed into the Kubelka–Munk function ($F(R)$) calculated as $F(R) = (1 - R)^2/2R$, where R is the experimentally measured reflectivity coefficient of the samples [32].

3. Results

3.1. Investigation of the catalytic activity in CO oxidation by light-off method

Fig. 1 presents the dependences of the CO conversion on temperature for catalysts Pd(N)/CeO_2-T-450 °C (1), Pd(N)/CeO_2-P-450 °C (2), Pd(N + A)/CeO_2-T-450 °C (3), and Pd(N + A)/CeO_2-P-450 °C (4). All the catalysts of this series were calcined in air at the same temperature, 450 °C. The presented data show that the ceria synthesis method substantially affects the catalyst activity. The CeO_2 support itself exhibits activity in the CO oxidation only at $T > 300$ °C (the data are not presented) and so, the T_{50} value is 390 °C. This is higher by 270 °C than T_{50} for the least active catalyst. The activity of all catalysts does not change monotonically. The conversion vs. temperature curves are characterized by hills and dips. They are observed most clearly for the catalysts prepared without acetate ions and somewhat flattened over Pd(N + A)/CeO_2-T-450 °C and Pd(N + A)/CeO_2-P-450 °C catalysts. The activity of the Pd/CeO_2 catalysts with high surface area prepared by thermolysis (CeO_2-T) significantly depends on the palladium deposition

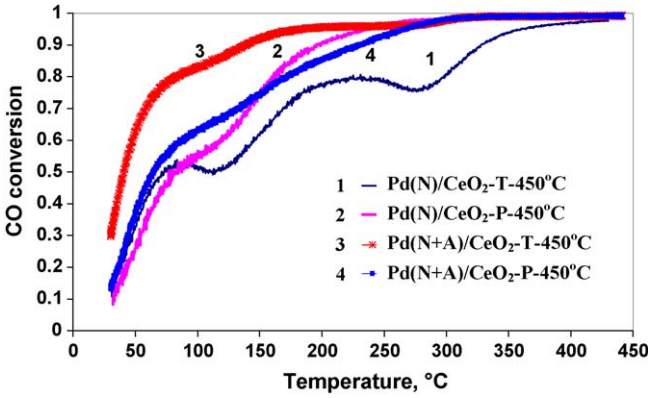

Fig. 1. Dependence of CO conversion on temperature over catalysts Pd(N)/CeO_2-T-450 °C (1), Pd(N)/CeO_2-P-450 °C (2), Pd(N + A)/CeO_2-T-450 °C (3) and Pd(N + A)/CeO_2-P-450 °C (4) oxidized in air.

method. The palladium deposition in the presence of acetate ions leads to more active catalysts (curves 1 and 3). The positive role of the acetate ions can be due to the better dispersion of palladium particles on the ceria surface and stronger interaction of palladium with the ceria surface resulting in the formation of the cationic palladium forms [33]. Meanwhile, the effect of acetic acid is almost non-existent for Pd/CeO_2 catalysts on the support prepared by precipitation (CeO_2-P). This may be due to the low surface area of the support and, consequently, low dispersity of the palladium particles on the support. A comparison of the catalysts synthesized over different supports and prepared using acetic acid shows that the activity of the sample with high surface area is higher that of the sample with low surface area, probably, due to better dispersion of the active component.

Fig. 2 presents the dependence of the CO conversion on temperature for these catalysts preliminary reduced in hydrogen. The presented results indicate that reduction in hydrogen results in a significant increase of the activity and changes of the shape of the CO conversion curve. It is interesting that the activity of the samples prepared without acetic acid is more affected by the reduction in hydrogen: T_{50} decreases by 25 °C. The activity of the samples prepared in the presence of acetic acid does not change much. For Pd(N + A)/CeO_2-T-450 °C T_{50} grows by 5 °C, whereas for Pd(N + A)/CeO_2-P-450 °C it decreases by 9 °C. These light-off data indicate that reduced forms of the catalyst active sites play a significant role in the mechanism of the low-temperature oxidation, in particular, for the light-off process.

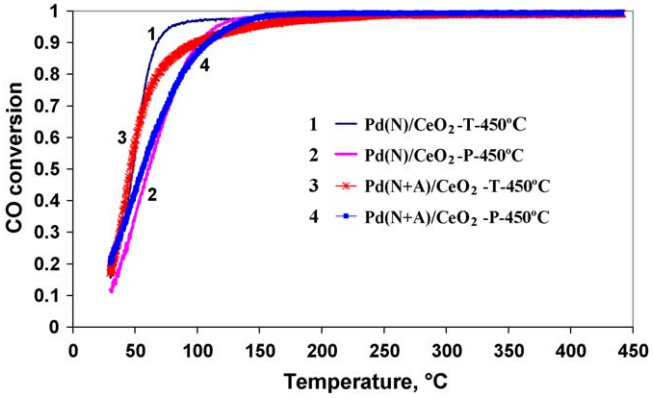

Fig. 2. Dependence of CO conversion on temperature over catalysts Pd(N)/CeO_2-T-450 °C (1), Pd(N)/CeO_2-P-450 °C (2), Pd(N + A)/CeO_2-T-450 °C (3) and Pd(N + A)/CeO_2-P-450 °C (4) reduced in H_2.

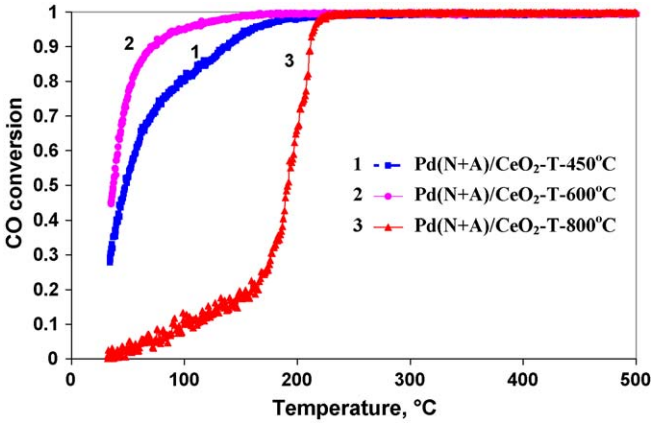

Fig. 3. Dependence of CO conversion on temperature over catalysts Pd(N + A)/CeO_2-T-450 °C (1), Pd(N + A)/CeO_2-T-600 °C (2) and Pd(N + A)/CeO_2-T-800 °C (3).

A comparison of the activity for samples prepared by different methods shows that the most active catalysts were prepared in the presence of acetic acid over ceria synthesized by thermolysis and characterized by high surface area of the support. In order to observe the changes of the low-temperature activity depending on the sintering of the support, CeO_2-T-450 °C support was also calcined at 600 and 800 °C. The dependences of the CO conversion on temperature for Pd(N + A)/CeO_2-T catalysts prepared using supports calcined at different temperatures are shown in Fig. 3. The support calcination at 600 and 800 °C decreases its surface area from 87 to 47 and 3 m^2/g, respectively. The increase of the support calcination temperature to 600 °C leads to a slight growth of the catalytic activity in the low-temperature range for the catalyst Pd(N + A)/CeO_2-T, so that its T_{50} decreases by 12 °C. Meanwhile, the calcination at 800 °C substantially decreases the catalytic activity, and T_{50} grows from 48 to 192 °C. As a result, the low-temperature activity of the catalyst synthesized on the sintered support is negligible. The maximum conversion is reached at ca. 200 °C. This is typical of CO oxidation over catalysts with the active component in the form of dispersed PdO particles [15].

3.2. Investigation of the catalysts by TPR-CO

The effect of calcination temperature on the state and reactivity of the active component was studied by TPR-CO. Fig. 4 shows the TPR-CO curves for samples Pd(N + A)/CeO_2-T-450 °C, 600 °C, 800 °C and for support CeO_2-T-450 °C. There are three maxima on the TPR curve of the Pd(N + A)/CeO_2-T-450 °C catalyst with T_{max} = ca. 70 °C (peak I), ca. 270 °C (wide peak II) and ca. 450 °C (peak III). Peak III can be attributed to CO reaction with oxygen from ceria because T_{max} of peak III matches T_{max} of pure ceria (Fig. 4, curve 4). The observation of CO consumption peaks at different temperatures indicates that the oxygen atoms of the catalyst are not equivalent with respect to bond energies. The first two peaks are related to both palladium and the support whereas the third one is related only to the support.

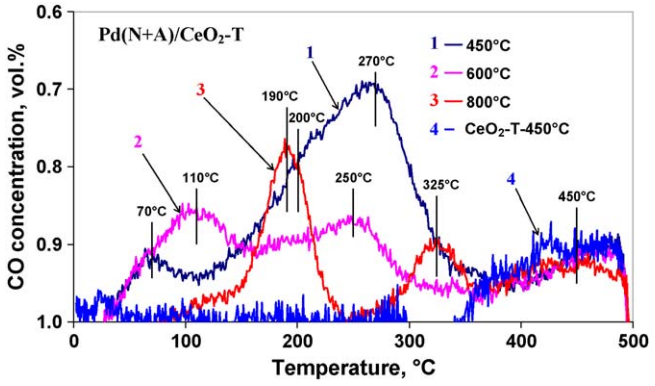

Fig. 4. TPR-CO spectra (dependence of CO concentration on temperature inverted relative to *Y*-scale) for catalysts Pd(N + A)/CeO_2-T-450 °C (1), Pd(N + A)/CeO_2-T-600 °C (2), Pd(N + A)/CeO_2-T-800 °C (3) and CeO_2-T-450 °C (4).

Three TPR peaks with T_{max} = ca. 110 °C, ca. 250 °C and ca. 450 °C and two unresolved shoulders with $T \sim 70$ and 200 °C overlapping peaks I and II were observed for the catalyst supported on CeO_2 preliminary calcined at 600 °C. Note that T_{max} of the first two peaks and their areas changed for this sample. T_{max} of peak I shifted to higher temperatures from 70 to 110 °C due to the growth of a new state, so that the area of this peak significantly increased. T_{max} of the second peak slightly decreased from 270 to 250 °C, whereas the area of this substantially decreased. It appears that more active sites with lower oxygen bond energy are formed over the support calcined at 600 °C. Thus, the increase of the fraction of particles with lower oxygen bond energy leads to the growth of the catalyst activity in CO oxidation for the sample calcined at 600 °C.

Further increase of the support calcination temperature to 800 °C results in the disappearance of type I and type II active sites accompanied by the formation of new sites with T_{max} = 190 °C. This implies that this sample does not have weakly bound oxygen. Consequently, T_{50} in CO oxidation shifts to higher temperatures as it is observed in the light-off curves (Fig. 3). Note that the sites of types I and II disappear together. This fact might indicate that the oxygen forms giving these two peaks in TPR-CO are interrelated. In other words, the formation of weakly bound oxygen (peak I) is due to the presence of a surface phase in which there are more strongly bound oxygen atoms (peak II).

3.3. XRD study of the catalysts

According to the XRD data (Table 1), in the samples supported on CeO_2-T calcined at 450 °C ceria exists as c-CeO_2 phase (a = 5.411 Å) with the average particles size of ca. 9 nm. Meanwhile, in the samples supported on CeO_2-P calcined at 450 °C the average size of the c-CeO_2 particles is larger, ca. 16 nm. No phases of Pd metal or PdO were observed in either sample.

3.4. XPS study of the catalysts

The spectra of Pd3d lines for samples Pd(N)/CeO_2-T-450 °C (Spectrum 1), Pd(N)/CeO_2-P-450 °C (Spectrum 2), Pd(N + A)/CeO_2-T-450 °C (Spectrum 3), Pd(N + A)/CeO_2-P-450 °C (Spectrum 4) calcined in air at 450 °C are shown in Fig. 5. The Pd3d spectra are presented as the difference spectra obtained by subtraction of Shierly's background from experimental spectra. The difference

Table 1
Physico-chemical properties of the Pd/CeO_2 catalysts.

Catalyst	Phase composition	Support calcination temperature (°C; duration, h)	$S_{specific}$ (m^2/g)
Pd(N)/CeO_2-T	c-CeO_2 with particle size 9.5 nm.	450 (4 h)	87
Pd(N+A)/CeO_2-T	PdO phase was not revealed.	600 (4 h)	47
		800 (4 h)	3
Pd(N)/CeO_2-P	c-CeO_2 with particle size 16 nm.	450 (4 h)	17
Pd(N+A)/CeO_2-P	PdO phase was not revealed.	600 (4 h)	14
		800 (4 h)	4

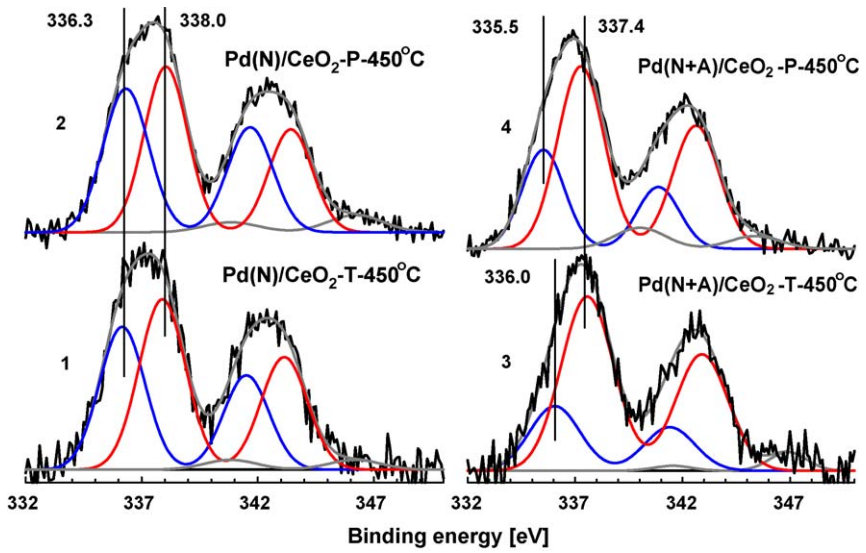

Fig. 5. Pd3d spectra of catalysts Pd(N)/CeO_2-T-450 °C (1), Pd(N)/CeO_2-P-450 °C (2), Pd(N + A)/CeO_2-T-450 °C (3) and Pd(N + A)/CeO_2-P-450 °C (4) after calcination at 450 °C in air.

spectra are shown together with the results of their decomposition into components using Voigt functions as a sum of Gaussian and Lorentzian curves. Equally with Voigt functions, the Doniach–Sunjic functions are widely used for curve fitting analysis in XPS [27]. Our curve fitting analysis showed that Voight functions are more compatible for the decomposition of experimental spectra. The curve fitting shows that Pd3d spectra of all samples consist of two main doublets characterizing palladium atoms in different oxidation states. The other components are caused by plasmon excitations and were added to obtain the description quality [34]. First of all, note that neither of the doublets can be attributed to palladium oxide particles because their positions are quite different from the value typical of PdO (336.8 ± 0.2 eV) [17,20,35]. Furthermore, there is no plasmon peak typical of PdO that should be located near 345 eV. Additionally, the electron microscopy data and the results obtained by UV–vis DRS that will be reported below also do not support the formation of PdO particles on the surface of the studied catalysts.

The doublet with a higher binding energy of spin–orbital components ($E_b(Pd3d_{5/2})$ = 337.4 eV (curves 3 and 4); 338.0 eV (curves 1 and 2)) can be attributed to palladium in the surface interaction phase (SIP) where the active component interacts with the supports surface (hereafter denoted as SIP or $Pd_xCeO_{2-\delta}$) [20,36]. Meanwhile, the other doublet with a lower E_b corresponds to palladium metallic clusters and nanoparticles. The attribution of the line with $E_b(Pd3d_{5/2})$ = ca. 337.4–338.0 eV to the surface palladium–ceria interaction phase $Pd_xCeO_{2-\delta}$ appears to be more reasonable compared to the hypothesis about the formation of oxides such as PdO_2 [24–26] that are unstable at high calcination temperatures.

Comparison of the Ce3d spectra also gives evidence to the formation of SIP rather than higher palladium oxide. Fig. 6 presents the normalized Ce3d spectra obtained from the calcined catalyst and support. Ce3d spectra are shown in the difference variant when spectral background is subtracted. These Ce3d spectra are presented in a standard variant of their deconvolution to components related to Ce^{3+} and Ce^{4+} ions according to [17,37,38]. The labeled components U, V, U″, V″, U‴, and V‴ are related with different final states of photoionized Ce^{4+}. Other four components U^0, V^0, U′, and V′ are assigned to Ce^{3+}. The concentration ratio of these ions in the surface layers was calculated from the corresponding component areas. It was found that the relative concentration of Ce^{3+} ions decreased from 25 to 20% after the palladium deposition. This decrease was readily reproducible for all samples and well beyond the experimental error. Based on these data, the decrease of the relative concentration of Ce^{3+} ions can be related to the interaction of the support surface with the palladium nitrate solution followed by partial reduction of Pd^{2+} ions to Pd metal and oxidation of the Ce^{3+} ions contacting with it. It should be mentioned that the $Ce(NO_3)_3$ thermolysis method used for the synthesis of this support yields a product with relatively high concentration of Ce^{3+} ions on the surface even despite calcination in air at relatively high temperature 450 °C. This fact proves that the catalyst surface and subsurface layers are highly defective. This defectiveness is related to the high concentration of Ce^{3+} ions and, therefore, oxygen vacancies.

Comparison of the Pd3d spectra of the samples Pd(N)/CeO_2-T-450 °C and Pd(N)/CeO_2-P-450 °C after calcination (Fig. 5) shows that the positions of the spectral components and their ratio are about the same. This fact proves that at relatively low palladium concentrations its deposition on the surface of supports with considerably different surface areas using the same deposition procedure results in approximately the same distribution of the palladium oxidation states.

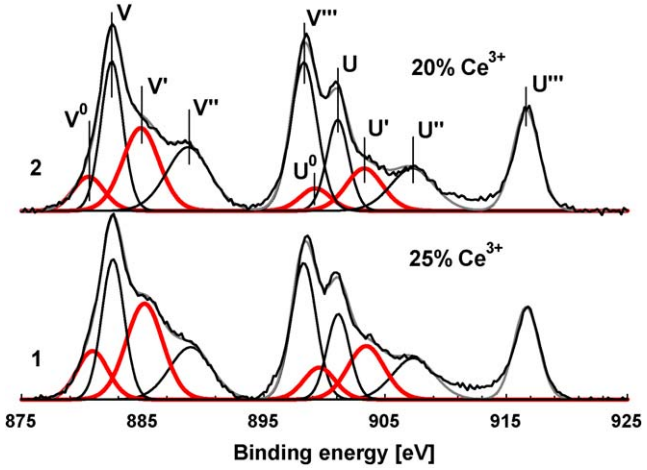

Fig. 6. Ce3d spectra of CeO_2-T-450 °C support (1) and supported catalyst Pd(N)/CeO_2-T-450 °C (2).

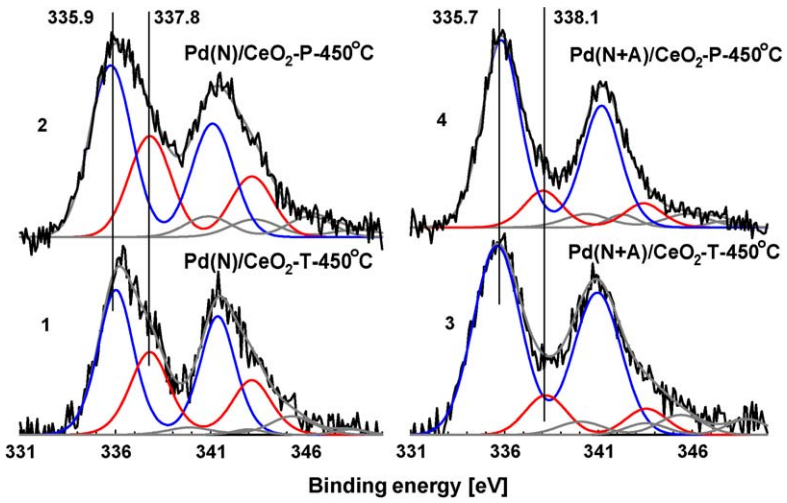

Fig. 7. Pd3d spectra of catalysts Pd(N)/CeO_2-T-450 °C-H_2 (1), Pd(N)/CeO_2-P-450 °C-H_2 (2), Pd(N + A)/CeO_2-T-450 °C-H_2 (3) and Pd(N + A)/CeO_2-P-450 °C-H_2 (4) after reduction in hydrogen at 450 °C.

When palladium was deposited in the presence of acetic acid, both the positions of Pd3d components and their relative intensities are changed. Both Pd3d doublets are shifted to lower binding energies. This fact indicates that palladium is more reduced in both phases, i.e. there is less oxygen in the SIP $Pd_xCeO_{2-\delta}$ and larger palladium metal particles are formed in this case.

In addition, the preparation procedure affects the Pd3d spectra of the samples reduced in hydrogen (Fig. 7). A higher palladium reduction degree was observed for samples Pd(N + A)/CeO_2-T-450 °C-H_2 (spectrum 3) and Pd(N + A)/CeO_2-P-450 °C-H_2 (spectrum 4) as the intensity of the doublet with $E_b(Pd3d_{5/2}) \sim 338$ eV considerably decreased and position of 'nanometallic' Pd3d doublet is more close to position of palladium in the bulk ($E_b(Pd3d_{5/2}) \sim 335.3$ eV [9,29,31,35,38]). Also $E_b(Pd3d_{5/2})$ for reduced palladium in these samples was somewhat lower than the corresponding value for samples Pd(N)/CeO_2-T-450 °C-H_2 (spectrum 1) and Pd(N)/CeO_2-P-450 °C-H_2 (spectrum 2) indicating that the palladium metal particles were larger in the former samples. These results prove that the catalysts prepared using acetic acid are not only better dispersed, but have higher lability relative to palladium redox processes in the interaction phase on the ceria surface.

Fig. 8 shows the Pd3d spectra of Pd(N + A)/CeO_2-T catalysts prepared using supports calcined at different temperatures (450 °C (1), 600 °C (2) and 800 °C (3)). Two doublets with $E_b(Pd3d_{5/2}) \sim 336.0$ and 337.7 eV were observed in the Pd3d spectra of the samples with the support calcined at 450 and 600 °C. As discussed above, these doublets can be attributed to small palladium metal particles and the interaction phase $Pd_xCeO_{2-\delta}$, respectively. Note that the increase of the support calcination temperature leads to an increase of the fraction of palladium metallic clusters. Meanwhile, the negligible shift for the doublet with $E_b(Pd3d_{5/2}) \sim 336.0$ eV allows suggesting that no sintering of palladium metallic particles occurs. In the meantime, the doublet attributed to the interaction phase is shifted by ca. 0.4 eV, indicating the palladium in this phase becomes more ionic. Thus, the support calcination at higher temperature (600 °C instead of 450 °C) results in a more homogeneous distribution of palladium metallic clusters on the surface of the interaction phase containing more oxygen.

Only one doublet with $E_b(Pd3d_{5/2}) = 336.9$ eV was observed in the Pd3d spectrum of the catalyst prepared using the support calcined at 800 °C. Its position matches well the position of the line in PdO in agreement with our experimental and literature data [17,20,36]. In addition, a plasmon peak at ca. 345.5 eV that is reliably attributed to the PdO phase [20] was also observed in this spectrum. The attempts to decompose the Pd3d line into two or more doublets were not successful. The most reliable and correct curve fitting is presented in Fig. 8 (spectrum 3).

Thus, preliminary annealing of the supports with crystallization of CeO_2 particles results in the lack of the interaction phase and active sites related to weakly bound oxygen responsible for the low-temperature catalytic activity in the catalyst prepared using this support.

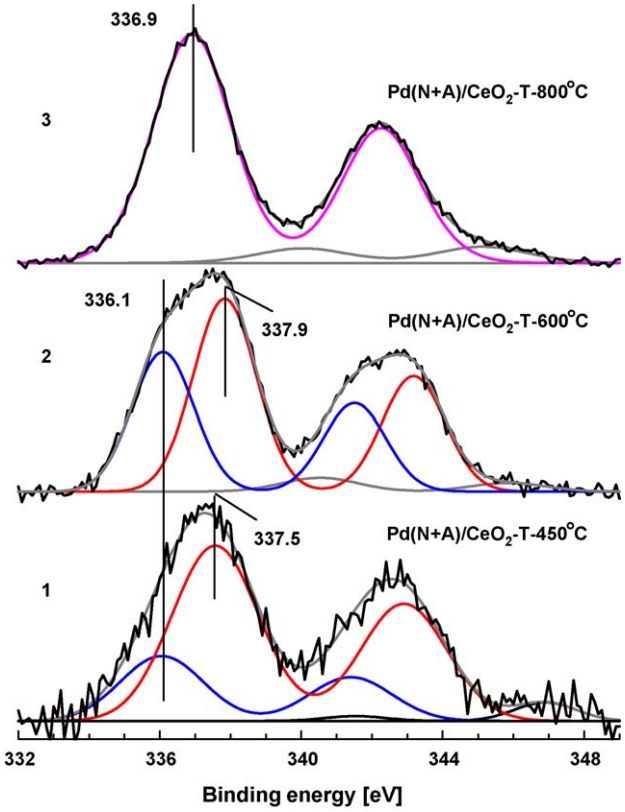

Fig. 8. Pd3d spectra of catalysts Pd(N + A)/CeO_2-T-450 °C (1), Pd(N + A)/CeO_2-T-600 °C (2) and Pd(N + A)/CeO_2-T-800 °C (3) after calcination of the support at the corresponding temperature in air.

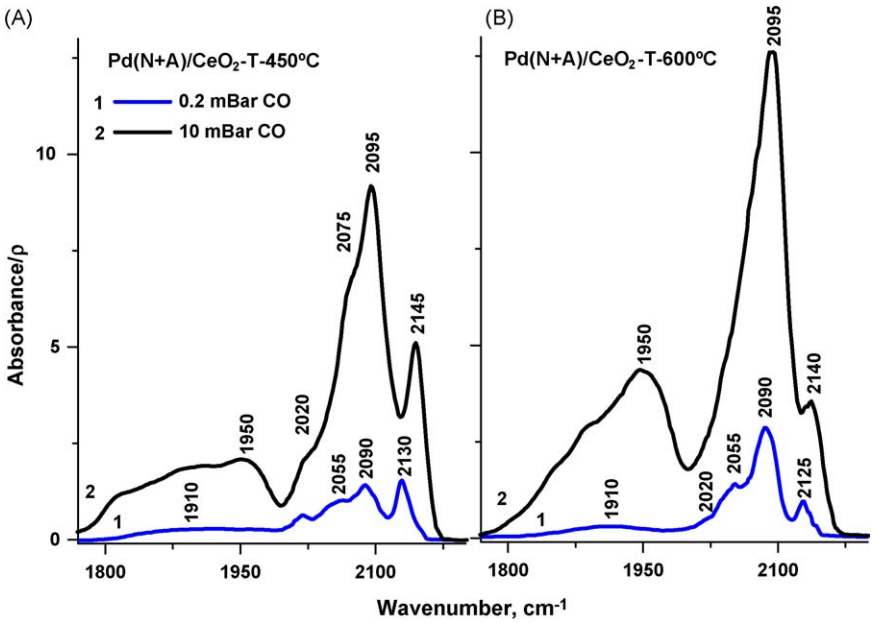

Fig. 9. FTIR spectra in the carbonyl region of CO adsorbed on Pd(N + A)/CeO_2-T-450 °C (A) and Pd(N + A)/CeO_2-T-600 °C (B) catalysts at 25 °C and CO pressure: curves 1—0.2 mBar and curves 2—10 mBar.

3.5. FTIR study of the catalysts

The surface state of the Pd particles supported on the CeO_2-T-450 °C and CeO_2-T-600 °C was studied by FTIR spectroscopy of adsorbed CO molecules. Only a weak absorption band (a.b.) at 2180 cm^{-1} was observed in the spectra of CO adsorbed at 25 °C on the surface of the supports. So, FTIR spectroscopy can be used for identification of the ionic and metal states of palladium in supported catalysts.

The FTIR spectra of CO adsorbed on Pd(N + A)/CeO_2-T-450 °C and Pd(N + A)/CeO_2-T-600 °C are shown in Fig. 9a and b. The following a.b. appeared when CO was adsorbed: 2140–2145, 2130–2125, 2090, 2055, 2020, 1950, 1910 and 1820–1840 cm^{-1}. The adsorption band at 1820–1840 cm^{-1} can be attributed to threefold-hollow CO species, the bands at 1910 and 1950 cm^{-1}—to bridged CO species, whereas the band at 2020–2095 cm^{-1} can be assigned to linear CO species on Pd metal particles [39,40]. The intensity of absorption bands of linear CO species substantially exceeds that of the bridged forms.

The intensity of a.b. at 2020 cm^{-1} increased with CO pressure and did not change after brief evacuation at 25 °C. Earlier a.b. at 2010–2020 cm^{-1} observed for reduced samples Pd/CeO_2-T calcined at 450 and 600 °C was ascribed to CO linearly bonded to a Pd atom in an electron-donor oxygen vacancy or to Pd sites with electronic properties strongly changed by interaction with basic oxide ions of the support [41]. The band at 2090 cm^{-1} only slightly shifted to higher frequencies (2095 cm^{-1}) when the CO pressure was increased. According to [42], this band can be attributed to linear CO complexes with palladium in an electron-deficient state. This electron deficiency on the metal can originate from the interaction of the metal particle with local sites of the support surface. This band can be easily removed by brief evacuation. The bands at 2055–2075 cm^{-1} did not disappear after brief evacuation and can be ascribed to CO linearly bonded to Pd atoms on edges, steps, and terraces of (1 0 0) and (1 1 1) facets [43].

The band at 2130–2125 cm^{-1} was observed on admission of 0.2 mbar CO. New absorption bands appeared at 2140–2145 cm^{-1} at the increase of CO pressure to 10 mbar. The a.b. could not be removed by brief evacuation at 25 °C. These bands can be assigned to CO adsorbed on two different Pd^{2+} species [44–46] probably, in the $Pd_xCeO_{2-\delta}$ phase.

Thus, in our system there are small disordered Pd metal particles strongly interacting with the support and palladium ions located in a finely dispersed amorphous interaction phase $Pd_xCeO_{2-\delta}$.

Comparison of the intensities of adsorbed CO bands on samples Pd(N + A)/CeO_2-T-450 °C and Pd(N + A)/CeO_2-T-600 °C shows that higher concentration of ionic state of palladium can be obtained using the support with lower calcination temperature (CeO_2-T-450 °C) because the intensities of a.b. at 2130 and 2145 cm^{-1} are much higher in the spectra of CO adsorbed on Pd(N + A)/CeO_2-T-450 °C. The electron-donor effect of the support on palladium metal particles is more significant for CeO_2-T-450 °C support. The intensity of the band at 2020 cm^{-1} in the spectra of adsorbed CO is greater on this support. Meanwhile, palladium particles formed on CeO_2-T-600 °C support are characterized by greater electron acceptor effect of the support because a more intense a.b. at 2095 cm^{-1} is observed in the spectra of adsorbed CO.

3.6. HRTEM studies

The particle morphology in samples Pd(N + A)/CeO_2-T-600 °C and Pd(N + A)/CeO_2-T-800 °C is presented in Figs. 10a–b and 11a–b, respectively. The size of CeO_2 crystallites in the sample calcined at 600 °C is 10–40 nm. After calcination at 800 °C they grow to 100 nm and more. The EDX spectra from CeO_2 particles in both samples reveal the presence of palladium (Fig. 12a and b). Meanwhile, the HRTEM images show that most Pd in the sample Pd(N + A)/CeO_2-T-600 °C is not usually observed (Fig. 10b). Only few Pd metal nanoparticles (clusters) with sizes of ca. 1 nm are observed on the CeO_2 surface (Fig. 10c). The Pd particles were identified using interplanar spacing $d_{1\,1\,1}$ = 0.224 in the images of their lattice obtained by HRTEM. An FFT picture (Fig. 10e) obtained from the HRTEM image of Pd cluster on CeO_2 (Fig. 10c and d) suggests epitaxial correspondence of the Pd and CeO_2 cubic lattices. For example, Fig. 10d shows a good match of the crystallographic directions [1 1 1] in the metal and oxide lattices with small angular disorientation (ca. 10 °) and the formation of more structures. The contrast of Pd particles at the background of

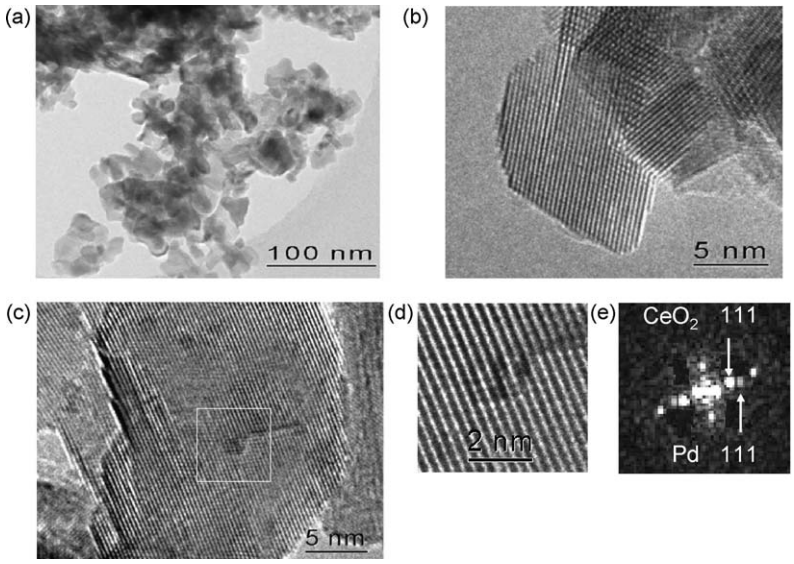

Fig. 10. TEM images of Pd(N + A)/CeO_2-T-600 °C catalyst: (a) morphology of CeO_2 support; (b) HRTEM image of CeO_2 particles, Pd particles are not visible; (c) Pd clusters with size about 1 nm; (d) single Pd cluster bound epitaxially with CeO_2; (e) FFT from cluster (arrows show patterns from Pd and CeO_2).

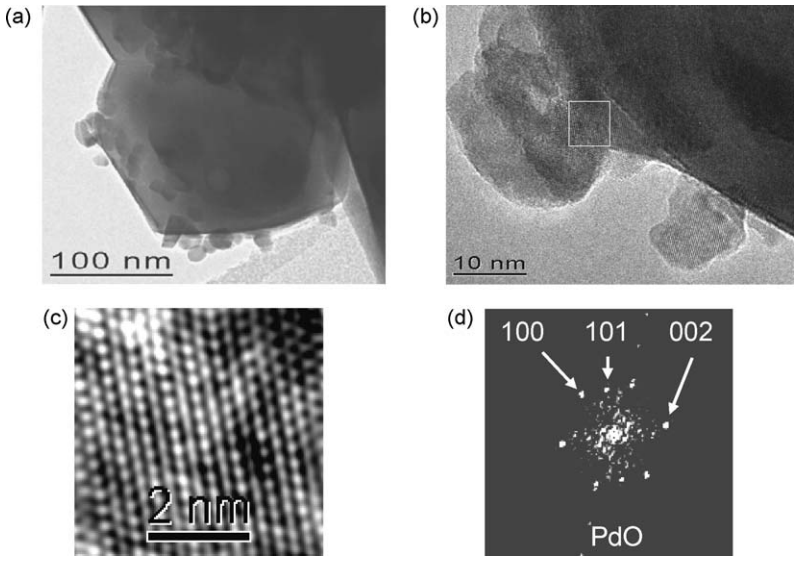

Fig. 11. TEM images of Pd(N + A)/CeO_2-T-800 °C catalyst: (a) PdO particles on the surface of CeO_2; (b) enlarged image of PdO particles (position for FFT is marked by frame); (c) HRTEM image of PdO lattice in [0 1 0] direction; (d) FFT with indication of patterns from PdO.

CeO_2 particles is rather poor. This may be caused by flattening of the palladium clusters due to strong epitaxial interaction of the metal with ceria. The most finely dispersed Pd form (isolated atoms or ions) is not observed in the HRTEM images. Nevertheless, the Pd observation by EDX in the sample without association of the atoms into Pd metal particles suggests that atomically dispersed Pd ions are stabilized in the surface layers of CeO_2.

Fig. 11a and b show that the sintering of the CeO_2 support in the Pd(N + A)/CeO_2-T-800 °C sample leads to the formation of many large three-dimensional crystalline PdO particles with sizes 10–20 nm. An EDX spectrum from PdO particle on ceria is shown in Fig. 12b. Fig. 11b shows that all the particles are composed of blocks. Fig. 11c shows a [0 1 0] projection of the crystalline lattice from a large PdO particle (from the fragment marked in Fig. 11b). The FFT picture (Fig. 11d) was identified as PdO phase. A PdO epitaxy on CeO_2 was not observed by HRTEM for this sample. So, only random physical interaction of large particles occurs.

Thus, the support calcination at 800 °C leads to substantial changes in the structure of Pd/CeO_2 sample. Large PdO particles are formed instead of finely dispersed atomic (ionic) or cluster Pd forms observed on the supports calcined at 450 and 600 °C.

3.7. UV–vis spectroscopy study

Fig. 13 presents the UV–vis spectra of Pd(N + A)/CeO_2-T catalysts prepared using ceria supports calcined at different temperatures. The spectra of the supports after calcination at the corresponding temperatures that were used as the background and difference spectra are shown for comparison. Two intense absorption bands at 37,000 and 29,300 cm^{-1} were observed for all the samples. They may be caused by $Ce^{4+} \leftarrow O^{2-}$ charge transfer and interband transitions in CeO_2 [47]. The declining branch of the band at 29,300 cm^{-1} from the short-wave side is responsible for the spectral background to transitions related to Pd. Two more a.b. in the visible region at 21,700 and 25,000–25,800 cm^{-1} were

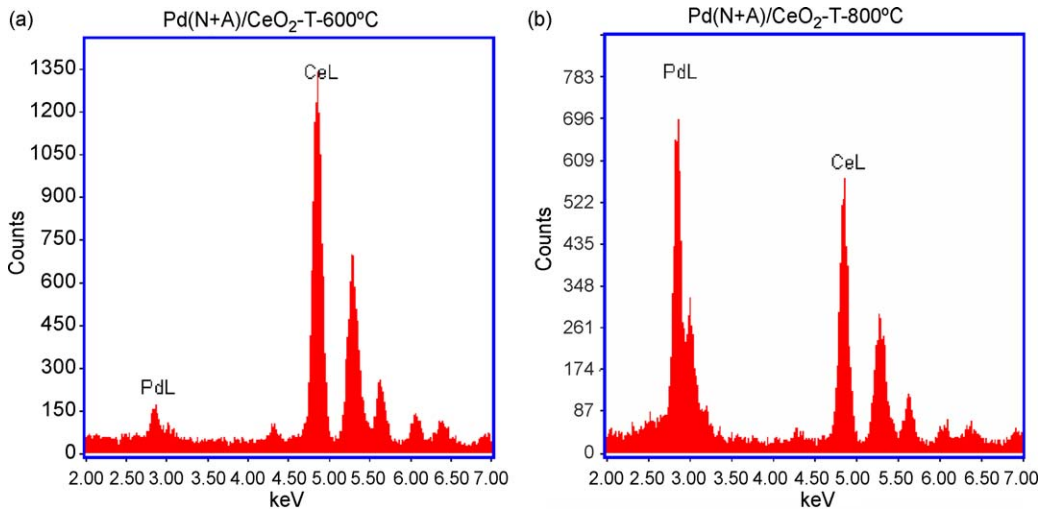

Fig. 12. (a) Sample Pd(N + A)/CeO_2-T-600 °C. EDX spectrum from CeO_2 particle, where Pd particles are not visible at the HRTEM image (Fig. 10b); (b) sample Pd(N + A)/CeO_2-T-800 °C. EDX spectrum from PdO particle located on CeO_2 (Fig. 11b).

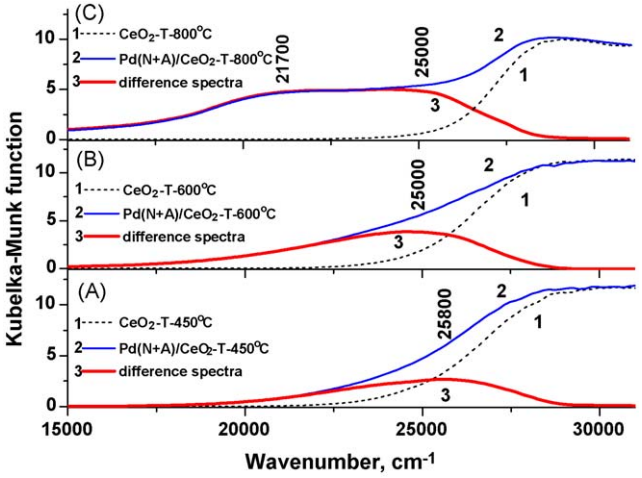

Fig. 13. UV–vis DR spectra of Pd(N + A)/CeO_2-T catalysts prepared using CeO_2 support calcined at different temperatures: 450 °C (A), 600 °C (B), 800 °C (C). 1—spectra of CeO_2 supports; 2—spectra of Pd/CeO_2 catalysts; 3—the difference spectra.

observed in the spectra of the catalysts. The band at 21,700 cm^{-1} was observed only for sample Pd(N + A)/CeO_2-T-800 °C. According to [48,49], a.b. at 21,000–22,000 cm^{-1} observed for aqueous solutions of palladium halides, e.g. $[PdCl_4]^{2-}$, corresponds to the spin-allowed d–d transitions in Pd^{2+} ions. When chloride ions were substituted for stronger ligands, such as H_2O, the band of d–d transitions in Pd^{2+} ions shifted to shorter wavelengths (ca. 25,000 cm^{-1} for $[Pd(H_2O)_4]^{2+}$) [49]. The band at 22,000 cm^{-1} was observed for a series of palladium catalysts supported on alumina [50]. The authors suggested that O^{2-} and Cl^- ions create crystalline fields of similar strengths in Pd^{2+} complexes because the same band was observed in the UV–vis spectra of the samples with and without chlorine ions. So, the intense absorption band at 21,700 cm^{-1} in the spectrum of Pd(N + A)/CeO_2-T-800 °C can be attributed to d–d transitions in Pd^{2+} ions in square-planar PdO complexes. The charge transfer bands in Pd^{2+} ions are overlapped by more intense a.b. of the support. Note that the band at 21,700 cm^{-1} was not observed in the spectra of the samples Pd(N + A)/CeO_2-T-450 °C and Pd(N + A)/CeO_2-T-600 °C. This fact appears to indicate that PdO phase is not present in these samples. The absorption band at 25,000–25,800 cm^{-1} can be assigned to d–d transitions in Pd^{2+} ions in stronger crystalline field, probably in a mixed $Pd_xCeO_{2-\delta}$ phase.

4. Discussion: factors determining LTA in CO oxidation

4.1. Formation, properties and role of surface interaction phase

The investigation of the catalytic and physicochemical properties of the synthesized Pd/CeO_2 samples showed that their LTA depends on many factors. The most important one is the interaction of the active component with the support. According to the XPS, FTIR and UV–vis data, there are several forms of palladium on the ceria surface. SIP is the strongest interaction that is characterized by $E_b(Pd3d_{5/2})$ = 337.7–338.2 eV in the XPS spectra. This value of $E_b(Pd3d_{5/2})$ is attributed to Pd^{2+}. Concerning the cerium state in SIP, it is problematic to determine unambiguously the oxidation state of cerium in this phase (Ce^{3+} or Ce^{4+}) from the Ce3d spectra. The reason is the low palladium concentration on the catalyst surface. So, it is very difficult to separate cerium atoms interacting with the palladium from the majority of cerium atoms in the support. The presence of a high-energy state in the Pd3d spectrum is typical only of supported palladium catalysts where the support is characterized by variable oxidation state of the metal ions that can be reduced relatively easily [20,23,24,36]. On the contrary, palladium with high binding energy is not formed at moderate calcination temperatures over oxides with constant oxidation state and strong M–O bonds (SiO_2, Al_2O_3). Usually, particles of the oxidized phase PdO are formed on such supports [10,51], and no LTA in CO oxidation is observed. The SIP formation requires the support oxide with variable oxidation state to be in a nanosized state with high surface defectiveness. The results presented in this paper in Figs. 3, 4, 8 and 10–13 unambiguously show that crystallization of the support and ordering of its surface by thermal treatment prevent strong interaction of palladium with the CeO_2 surface. Evidently, the adhesion heat is low on a well-crystallized and oxidized CeO_2 surface and does not facilitate the SIP formation. As a result, PdO nanoparticles, as another more thermodynamically stable phase of the active component, are formed in this case. Thus, to form SIP, the CeO_2 support has to be in a nanosized state that provides a defective disordered state of the surface. This defective state appears to increase the reducing ability of CeO_2, especially in the surface layers, providing for strong chemical interaction with palladium. The need for some reduction of the oxide surface to gain strong interaction with metals has been mentioned in several papers [7,24,52].

This nanosized state is not the only factor that controls the SIP formation. For instance, LTAs of the catalysts with different specific areas of supports CeO_2-T and CeO_2-P are not cardinally different. Moreover, the investigation of the catalytic activity showed that the behavior of the light-off curves can differ enough for catalysts prepared on the same support using different Pd deposition techniques. As noted above, it is also very important to deposit palladium from solution on the support surface in the very uniform and most finely dispersed form. The presence of acetate ions can help to reach this goal during palladium deposition.

So, the obtained results indicate that certain requirements have to be met both by the support and by the method used for deposition of the active component in order to form SIP. Highly defective surface of the support and very uniform palladium deposition in the most finely dispersed form are required to obtain active SIP.

It is difficult to make any conclusions on the stoichiometry of $Pd_xCeO_{2-\delta}$ SIP from the presented data. Taking into account the fact that palladium–ceria catalysts are active in wide temperature range, the composition of this phase apparently can be varied in a very wide range, and one Pd^{2+} ion can activate a significant number of oxygen atoms. We believe that the role of SIP is to activate oxygen of the support by increasing its mobility, making possible to use it efficiently at low temperatures. The SIP stoichiometry will be discussed later in the following papers devoted to the investigation of LTA on Pd–Ce systems.

4.2. Reduced state of palladium

The results obtained by XPS, FTIR and HRTEM indicate that a significant amount of palladium exists on the CeO_2 surface in reduced form. FTIR reveals the presence of reduced state Pd^0. The XPS data give two main characteristics of the electronic state of palladium: $E_b(Pd3d_{5/2}) = 337.8 \pm 0.3$–$338.2$ eV (palladium in SIP) and $E_b(Pd3d_{5/2}) = 336.0 \pm 0.3$ eV. As it was discussed above, the position of the latter peak is between the positions typical of Pd metal ($E_b = 335.2 \pm 0.2$ eV) and PdO ($E_b = 336.8 \pm 0.2$ eV) [7,9,10,13,14,16,27,31,34]. In the literature, the state with $E_b > 336$ eV is usually assigned to separate or interacting PdO particles. However, the results obtained by a complex of methods (TPR-CO, HRTEM, FTIR and UV–vis spectroscopy) bring us to the conclusion that no PdO particles are present on the surface of the catalysts having LTA.

Formally, the position of the peak of reduced palladium in the Pd3d spectrum corresponds to the oxidation state Pd^{1+}. However, the reduced state cannot be attributed only to the Pd^{1+} state because there is no separate metal state with $E_b = 335.2$ eV in the Pd3d spectrum. We believe that the low-energy doublet in the Pd3d spectra is related to palladium in the form of extremely small metal particles. The attribution of the doublet in the Pd3d spectrum with lower energies $E_b = 336.0 \pm 0.3$ eV to metal clusters is based on both the experimental and theoretical studies by photoelectron spectroscopy of metal clusters deposited on carriers and supports with different conductivities. In agreement with [53–55], the observed values $E_b(Pd3d_{5/2}) \sim 336.0$ eV, which exceed those typical of the palladium metal state ($E_b(Pd3d_{5/2}) \sim 334.8$–$335.4$ eV), can be explained by the size effects in the photoionization process of metal clusters. According to this concept, when metal clusters localized on an insulator carrier become smaller, the photolines of metal are shifted to higher binding energies due to the decrease of extra-atomic relaxation and charge conservation in the final state.

In addition, higher binding energies $E_b(Pd3d_{5/2}) \sim 335.7$–$336.0$ were also observed in the experimental study of catalysts reduced by hydrogen (Fig. 7) under conditions when palladium must be reduced to palladium metal. The reduction of palladium was confirmed by intensive hydrogen consumption. The reduced catalysts are also characterized by two components in the Pd3d spectra (Fig. 7). However, their main component is a doublet with $E_b(Pd3d_{5/2}) \sim 335.7$–$336.0$ eV characterizing palladium metal. A similar interpretation has also been suggested in the investigation of a Pd/Si_3N_4 system [56].

Thus, the spectroscopic data indicate that the reduced state of palladium in Pd/CeO_2 catalysts is composed of small islands of palladium metal. Apparently, the boundary atoms of the palladium islands undergo a strong polarizing effect from oxygen of the support. This effect can result in partial transfer of the electron density to the support to form partially charged boundary palladium atoms with oxidation state close to Pd^{1+}. In the case of small metal particles, the contribution of the boundary palladium atoms to the total number of atoms in the particle can be relatively high and affect the chemical shift of palladium photoelectron lines in the XPS spectra.

The electron microscopy data can be interpreted using the same approach. According to the HRTEM and EDX data, the surface of catalysts prepared using supports calcined at 450 and 600 °C contains small palladium metal particles in addition to atomically dispersed palladium. These particles are epitaxially bound to the CeO_2 surface. In this case, the electron density can be transferred from palladium to the surface of the support to form a charged metal particle. The epitaxial bonding of palladium to the support surface results in a substantial electron and structural modification of palladium leading to the formation of small flat two-dimensional palladium clusters. The formed two-dimensional palladium structures appear to be most suitable for optimal CO activation and subsequent formation of reaction intermediates. Due to the epitaxial interaction, this state of palladium can be relatively stable with respect to oxygen and resist the formation of PdO particles. Under the action of the reaction mixture and growing temperature the epitaxially bound islands can probably be transformed to other palladium–ceria structures. However, these transformations are reversible and do not lead to three-dimensional PdO structures. It is clear that thermal stability of the catalysts to low-temperature CO oxidation is largely determined by the stability of two-dimensional palladium particles with respect to annealing to three-dimensional metal or oxide particles.

4.3. Effect of hydrogen on the formation of Pd/CeO_2 LTA catalysts

The data presented in Figs. 1 and 2 show that preliminary calcination of the catalysts in hydrogen has a significant activating effect on the LTA appearance. The CO conversion at low temperatures sharply increases and the maximum conversion is achieved at $T = 70$–120 °C. This effect can be stronger than certain fine details in the synthesis of the catalysts. This phenomenon can be related to two reasons.

The first one is the formation of the reduced palladium phase as small metal islands of optimal size. For instance, the XPS data (Figs. 5 and 7) show that after treatment in hydrogen the "metal" doublet in the Pd3d spectra is only slightly shifted to lower E_b, but it does not reach the value of 335.2 eV typical of large palladium metal particles. The E_b values observed for the four samples (Fig. 7) are in the interval 335.7–336.0 eV. These values appear to correspond to an optimum electronic and geometrical (size and shape) structure of palladium clusters required for CO oxidation at low temperatures. For comparison, the TPR-CO spectra give a reliable evidence of much stronger reduction of the active component during interaction with CO. These data agree with the results of Zhu et al. [57] who suppose that "the reason may be that the dissociation of adsorbed H_2 is necessary for the reduction by H_2, while CO can directly attack the surface oxygen in CeO_2 sample".

The second possible reason is the formation of specific hydroxyl groups located on the support either along the boundary with palladium islands or on the whole SIP surface. In any case, the OH^- group formed during the hydrogen treatment can affect the formation of the active component in certain electronic and structural state. They can also react with CO, forming the reaction intermediate such as hydrocarbonate or formate complexes. The effect of OH^- groups on the low-temperature CO oxidation has been reported in several papers in relation to PROX and WGS reactions [6,7,52,56].

5. Conclusion

The detailed investigation of palladium–ceria catalysts for low-temperature CO oxidation was carried out by a complex of physicochemical and kinetic methods. HRTEM and EDX methods showed that the catalysts having low-temperature activity are characterized by extremely high palladium dispersion on the surface of the supports. XPS revealed two different states of palladium composed of the SIP $Pd_xCeO_{2-\delta}$ and small metal clusters ($d < 10$ Å). The diffraction images obtained by HRTEM show that these clusters have flattened shape due to epitaxial bonding between (1 1 1) facets of palladium and CeO_2. FTIR distinguished two types of CO adsorption sites (Pd^{2+} and Pd^0) that can be related to SIP (Pd^{2+}) and palladium metal clusters (Pd^0). The loss of LTA in CO oxidation is related to the loss of chemical interaction between palladium and the support followed by palladium sintering to large PdO nanoparticles. The presented results show unambiguously that PdO particles are not responsible for LTA in CO oxidation.

Thus, we have determined a two-phase structure of the active sites consisting of atomically dispersed palladium in SIP and palladium in metal nanoclusters. The catalysts pretreatment in hydrogen was found to significantly improve their catalytic (LTA) properties. The effect of hydrogen treatment was supposed to be related to the formation of hydroxyl groups. Effect of hydroxyl groups can be bound with the influence on the electronic and geometrical state of the surface active sites and their possible direct participation in the CO oxidation.

Acknowledgements

This study was supported by the Russian Foundation for Basic Research (Grants 07-03-07797 and 07-03-12218). The authors are grateful to E.M. Moroz for the XRD study of the samples.

References

[1] R.J. Farrauto, C.H. Bartholomew, Fundamentals of Industrial Catalytic Processes, Blackie, London, 1997, p. 265.
[2] G.C. Koltsakis, A.M. Stamatelos, Prog. Energy Combust. Sci. 23 (1997) 1.
[3] R. Craciun, W. Daniell, H. Knözinger, Appl. Catal. A: Gen. 230 (2002) 153.
[4] L. Li, Y. Zhan, Q. Zheng, Y. Zheng, X. Lin, D. Li, J. Zhu, Catal. Lett. 118 (2007) 91.
[5] S. Damyanova, C.A. Perez, M. Schmal, J.M.C. Bueno, Appl. Catal. A: Gen. 234 (2002) 271.
[6] A. Wootsch, C. Descorme, D. Duprez, J. Catal. 225 (2004) 259.
[7] O. Pozdnyakova, D. Teschner, A. Wootsch, J. Krohnert, B. Steinhauer, H. Sauer, L. Toth, F.C. Jentoft, A. Knop-Gericke, Z. Paál, R.J. Schlogl, J. Catal. 237 (2006) 17.
[8] H. Hea, H.X. Dai, C.T. Au, Catal. Today 90 (2004) 245.
[9] S.-H. Oh, G.B. Hoflund, J. Phys. Chem. A 110 (2006) 7609.
[10] S. Penner, P. Bera, S. Pedersen, L.T. Ngo, J.J.W. Harris, C.T. Campbell, J. Phys. Chem. B 110 (2006) 24577.
[11] H. Gabasch, W. Unterberger, K. Hayek, B. Klotzer, E. Kleimenov, D. Teschner, S. Zafeiratos, M. Havecker, A. Knop-Gericke, R. Schlogl, J. Han, F.H. Ribeiro, B. Aszalos-Kiss, T. Curtin, D. Zemlyanov, Surf. Sci. 600 (2006) 2980.
[12] G. Ertl, Adv. Catal. 37 (1990) 213.
[13] M. Bowker, I.Z. Jones, R.A. Bennett, F. Esch, A. Baraldi, S. Lizzit, G. Comelli, Catal. Lett. 51 (1998) 187.
[14] I. Jones, R. Bennett, M. Bowker, Surf. Sci. 439 (1999) 235.
[15] A. Bourane, D. Bianchi, J. Catal. 222 (2004) 499.
[16] S.-H. Oh, G.B. Hoflund, J. Catal. 245 (2007) 35.
[17] Parthasarathi Bera, K.C. Patil, V. Jayaram, G.N. Subbanna, M.S. Hegde, J. Catal. 196 (2000) 293.
[18] P. Mars, D.W. Van Krevelen, Chem. Eng. Sci. 3 (Spec. Suppl.) (1954) 41.
[19] Y. Nagai, T. Hirabayashi, K. Dohmae, N. Takagi, T. Minami, H. Shinjoh, S. Matsumoto, J. Catal. 242 (2006) 103.
[20] S. Roy, A. Marimuthu, M.S. Hegde, G. Madras, Appl. Catal. B: Environ. 73 (2007) 300.
[21] S. Suhonen, M. Valden, M. Pessa, A. Savimäki, M. Härkönen, M. Hietikko, J. Pursiainen, R. Laitinen, Appl. Catal. A: Gen. 207 (2001) 113.
[22] Xiaoping Cao, Lili Cao, Wenqing Yao, Xiaoyan Ye, Surf. Interf. Anal. 24 (1996) 662.
[23] M. Schmal, M.M.V.M. Souza, N.S. Resende, A.L. Guimaraes, C.A. Perez, J.G. Eon, D.A.G. Aranda, L.C. Dieguez, Catal. Today 100 (2005) 145.
[24] V. Matolrin, I. Matolrinovra, T. Mori, M. Yoshitake, J. Surf. Sci. Nanotechnol. 4 (2006) 497.
[25] E. Paparazzo, Surf. Sci. 234 (1990) L253.
[26] Limei Qiu, Fen Liu, Liangzhong Zhao, Ying Ma, Jiannian Yao, Appl. Surf. Sci. 252 (2006) 4931.
[27] D. Briggs, M. Seah (Eds.), Practical Surface Analysis by Auger and X-ray Photoelectron Spectroscopy, Wiley, Chichester, 1983.
[28] E.M. Slavinskaya, Yu.A. Chesalov, A.I. Boronin, I.A. Polukhina, A.S. Noskov, Kinet. Catal. 46 (2005) 555.
[29] A.I. Titkov, A.N. Salanov, S.V. Koscheev, A.I. Boronin, React. Kinet. Catal. Lett. 86 (2005) 371.
[30] A.S. Knyazev, O.V. Magaev, O.V. Vodyankina, A.I. Titkov, A.N. Salanov, S.V. Koshcheev, A.I. Boronin, Kinet. Catal. 46 (2005) 144.
[31] J.F. Moulder, W.F. Stickle, P.E. Sobol (Eds.), Handbook of X-ray Photoelectron Spectroscopy, Perkin-Elmer Corporation Physical Electronics Division, Eden Prairie, Minnesota, 1992.
[32] H.-P. Boehm, H. Knozinger, in: J.R. Anderson, M. Boudart (Eds.), Catalysis Science and Technology, 4, Springer-Verlag, Berlin-Heidelberg-New York, 1983, p. 39.
[33] W.-J. Shen, Y. Ichihashi, H. Ando, M. Okumura, M. Haruta, Y. Matsumura, Appl. Catal. A: Gen. 217 (2001) 165.
[34] Th. Pilloy, R. Zimmermann, P. Steiner, S. Hufner, J. Phys.: Condens. Matter 9 (1997) 3987.
[35] R.S. Monteiro, D. Zemlyanov, J.M. Storey, F.H. Ribeiro, J. Catal. 199 (2001) 291.
[36] Li-hua Xiao, Kun-peng Sun, Xian-lun Xu, Xiao-nian Li, Catal. Commun. 6 (2005) 796.
[37] M.A. Henderson, C.L. Perkins, M.H. Engelhard, S. Thevuthasan, C.H.F. Peden, Surf. Sci. 526 (2003) 1.
[38] E.L. Wilson, Q. Chen, W.A. Brown, G. Thornton, J. Phys. Chem. 111 (2007) 14215.
[39] N. Sheppard, T.T. Nguyen, in: R.I.H. Clark, R.E. Hester (Eds.), Advances in Infrared and Raman Spectroscopy, 5, Heyden, Philadelphia-Rheine, 1978, p. 67.
[40] J.B. Giorgi, T. Schroeder, M. Bäumer, H.-J. Freund, Surf. Sci. 498 (2002) L71.
[41] F. Prinetto, M. Manzoli, G. Ghiotti, M. de Jesus Martinez Ortiz, D. Tichit, B. Coq, J. Catal. 222 (2004) 238–249.
[42] A.Yu. Stakheev, L.M. Kustov, Appl. Catal. A: Gen. 188 (1999) 3.
[43] S. Bertarione, D. Scarano, A. Zecchina, V. Johanek, J. Hoffman, S. Schauermann, M.M. Frank, J. Libuda, G. Ruppechter, H.-J. Freund, J. Phys. Chem. B 108 (2004) 3603.
[44] K.I. Hadjiivanov, G.N. Vayssilov, Adv. Catal. 47 (2002) 307.
[45] D. Tessier, A. Rakai, F. Bozon-Verduraz, J. Chem. Soc. Faraday Trans. 88 (1992) 741.
[46] R. Craciun, W. Faniell, H. Knozinger, Appl. Catal. A: Gen. 230 (2002) 153.
[47] A. Bensalem, J.C. Muller, F. Bozon-Verduraz, J. Chem. Soc. Faraday Trans. 85 (1992) 153.
[48] A.B.P. Lever, Inorganic Electronic Spectroscopy, 2, Elsevier, Amsterdam-Oxford/NewYork-Tokyo, 1984, p. 491.
[49] L.I. Elding, L.F. Olsson, J. Phys. Chem. 82 (1978) 69.
[50] A.L. Tarasov, V.A. Shvets, A.V. Zaitsev, V.B. Kazanskii, Kinet. Catal. 27 (1986) 1022.
[51] K. Otto, L.P. Haack, J.E. deVries, Appl. Catal. B: Environ. 1 (1992) 1.
[52] M. Okumura, N. Masuyama, E. Konishi, S. Ichikawa, T. Akita, J. Catal. 208 (2002) 485.
[53] M.G. Mason, Z. Phys.: Phys. Rev. B 27 (1983) 748.
[54] Z. Bastl, Vacuum 36 (1985) 447–448.
[55] G.K. Wertheim, Condens. Matter 66 (1987) 53.
[56] I. Kurzina, F.J. Cadete Santos Aires, G. Bergeret, J.C. Bertolini, Chem. Eng. J. 107 (2005) 45.
[57] Huaqing Zhu, Zhangfeng Qin, Wenjuan Shan, Wenjie Shen, Jianguo Wang, J. Catal. 225 (2004) 267.